N6-Furfuryladenine is protective in Huntington's disease models by signaling huntingtin phosphorylation

Laura E. Bowie[a], Tamara Maiuri[a], Melanie Alpaugh[b], Michelle Gabriel[c], Nicolas Arbez[d], Danny Galleguillos[b], Claudia L. K. Hung[a], Shreya Patel[a], Jianrun Xia[a], Nicholas T. Hertz[e], Christopher A. Ross[d], David W. Litchfield[c], Simonetta Sipione[b], and Ray Truant[a,1]

[a]Department of Biochemistry and Biomedical Sciences, McMaster University, Hamilton, ON L8S 4L8, Canada; [b]Department of Pharmacology, University of Alberta, Edmonton, AB T6G 2R3, Canada; [c]Department of Biochemistry, Western University, London, ON N6A 3K7, Canada; [d]Division of Neurobiology, Department of Psychiatry and Behavioral Sciences, Johns Hopkins University School of Medicine, Baltimore MD 21205; and [e]Mitokinin, LLC, New York, NY 10006

Edited by Nancy E. Kleckner, Harvard University, Cambridge, MA, and approved June 19, 2018 (received for review January 31, 2018)

The huntingtin N17 domain is a modulator of mutant huntingtin toxicity and is hypophosphorylated in Huntington's disease (HD). We conducted high-content analysis to find compounds that could restore N17 phosphorylation. One lead compound from this screen was N6-furfuryladenine (N6FFA). N6FFA was protective in HD model neurons, and N6FFA treatment of an HD mouse model corrects HD phenotypes and eliminates cortical mutant huntingtin inclusions. We show that N6FFA restores N17 phosphorylation levels by being salvaged to a triphosphate form by adenine phosphoribosyltransferase (APRT) and used as a phosphate donor by casein kinase 2 (CK2). N6FFA is a naturally occurring product of oxidative DNA damage. Phosphorylated huntingtin functionally redistributes and colocalizes with CK2, APRT, and N6FFA DNA adducts at sites of induced DNA damage. We present a model in which this natural product compound is salvaged to provide a triphosphate substrate to signal huntingtin phosphorylation via CK2 during low-ATP stress under conditions of DNA damage, with protective effects in HD model systems.

DNA repair | oxidation | Huntington's disease | neurodegeneration | high-content analysis

Huntington's disease (HD) is a dominantly inherited neurodegenerative disorder characterized by late age-onset loss of cognition, emotional disorder, and loss of motor control. The disease is caused by a CAG expansion within the first exon of the *HTT* gene, which translates to a polyglutamine expansion in the huntingtin protein (1). Although the expansion of CAG length is correlated with age of disease onset, individuals with the same number of CAG repeats may vary in their disease onset by 40 y or more (2). Genome-wide association studies (GWAS) performed on large cohorts of HD patients to identify genetic modifiers of disease onset highlighted DNA-repair pathways, redox control proteins, and mitochondrial energy metabolism as the major modifiers of the onset of HD (3, 4). We have since defined huntingtin as a component of the ataxia telangiectasia mutated (ATM) DNA damage-response complex that accumulates at sites of DNA oxidative damage and as a scaffold for DNA-repair factors (5). Along with these newly defined functions, huntingtin has also previously been implicated in vesicular and axonal trafficking, cell division, synaptic transmission, and the cell stress response (6–11). Reflecting this variety of functions, the huntingtin protein localizes to several subcellular compartments. Localization is largely regulated by the first 17 amino acids of the protein, the N17 domain, which is phosphorylated at two key residues: serines S13 and S16 (12, 13).

The N17 domain, directly adjacent to the polyglutamine tract, forms an amphipathic α-helix that reversibly tethers huntingtin to membranes (7, 14), regulating intracellular localization between vesicles, the endoplasmic reticulum (ER), the primary cilium, and the nucleus (15). Huntingtin nuclear localization is primarily affected by cell stress (7), and the N17 domain is a reactive oxygen species (ROS) sensor, whereby sulfoxidation of the methionine M8 residue promotes the release of huntingtin from membranes, S13/S16 phosphorylation, and translocation to the nucleus (11). Deletion of the N17 domain accelerates disease in mouse and zebrafish models of HD (16, 17), implicating the domain in disease progression. In HD mouse models, serine phospho-mimetics (12) or induced serine phosphorylation (18) can prevent or fully reverse the toxicity of mutant huntingtin, defining restoration of N17 phosphorylation as a valid subtarget for HD therapeutic development.

We therefore set out to identify compounds that could modulate N17 phosphorylation in an attempt to restore the hypophosphorylation of N17 seen in HD cells (13, 19). Using an extensively validated antibody against phosphorylated S13 and S16 (13), we conducted a high-content screen for the effects of diverse small-molecule natural products on N17 phosphorylation. To minimize investigator bias, we used both blind, automated microscopy image acquisition and nonsupervised machine sorting of the images. We identified a number of compounds with known activities in the context of HD as well as one unique compound, N6-furfuryladenine (N6FFA), also known as "kinetin."

N6FFA has been extensively studied (20) and annotated as a plant cytokine with biological effects in mammalian cells, including

Significance

We have discovered a molecule derived from DNA-damage repair that can correct the lack of phosphorylation of mutant huntingtin, the cause of Huntington's disease (HD). In a mouse model, treatment reverses HD-like disease, and we see the lowering of mutant huntingtin levels to normal. The mechanism of this molecule is that it is processed to make a signal for kinase activity essential for repairing DNA. This mechanism is critical when neurons are stressed and have very low or absent energy levels. We propose that this molecule is a type of signaling from DNA-damage repair that occurs at dangerously low ATP levels.

Author contributions: L.E.B., T.M., M.A., M.G., N.A., S.S., and R.T. designed research; L.E.B., T.M., M.A., M.G., N.A., D.G., C.L.K.H., S.P., and J.X. performed research; T.M., M.A., M.G., N.A., D.G., C.L.K.H., S.P., J.X., and N.T.H. contributed new reagents/analytic tools; L.E.B., T.M., M.A., M.G., N.A., N.T.H., C.A.R., D.W.L., and R.T. analyzed data; and L.E.B., T.M., S.S., and R.T. wrote the paper.

Conflict of interest statement: R.T. is on the Scientific Advisory Board and is a minor shareholder of Mitokinin, LLC. N.T.H. is the Chief Scientific Officer of Mitokinin, LLC.

This article is a PNAS Direct Submission.

[1]To whom correspondence should be addressed. Email: truantr@mcmaster.ca.

This article contains supporting information online at www.pnas.org/lookup/suppl/doi:10.1073/pnas.1801772115/-/DCSupplemental.

Published online July 9, 2018.

protection against oxidative stress (21) and delay of age-related phenotypes in human fibroblasts (22). N6FFA is also a product of DNA oxidation by ROS (23) and occurs as a normal excreted human metabolite (24). N6FFA/kinetin was found to be the precursor to N6FFA/kinetin triphosphate (KTP), an ATP analog produced upon the salvaging of N6FFA by adenine phosphoribosyltransferase (APRT) (25). This nucleotide salvaging is important in the context of HD, where ATP levels are significantly reduced (26), particularly in neurons which rely heavily on nucleotide salvage as opposed to de novo nucleotide biosynthetic pathways (27, 28). Further, ATP production can halt during DNA-damage repair (29), and free ATP levels drop significantly during the ER stress response (9). Here, we show casein kinase 2 (CK2) can use KTP to phosphorylate N17 and that treatment with the N6FFA precursor molecule is protective in cell neuronal and animal models of HD.

We propose a model in which this natural product, upon being salvaged, potentiates the enzymatic phosphorylation reaction on polyglutamine-expanded huntingtin, allowing proper degradation of the mutant protein (30). In vivo administration of N6FFA, a blood–brain barrier (BBB)-permeable molecule (31), in HD model mice resulted in reduced cortical brain inclusions in YAC128 mice as well as HD phenotypic reversal.

Results

High-Content Analysis Identifies N6FFA as a Modulator of N17 Phosphorylation. Phosphorylation of huntingtin N17 at S13 and S16 has been shown to be a beneficial modification in the context of HD in both cell and animal models (12, 18). To identify modulators of N17 phosphorylation of huntingtin, we used high-content analysis to screen a library of 133 natural compounds (Selleckchem) for their potential effects on the fluorescent signal pattern of anti–N17-S13pS16p, an antibody recognizing N17 phosphorylated on S13 and S16. This antibody was raised to the phospho-S13/phospho-S16 epitope and was cross-purified by peptide-affinity chromatography both to the phospho-peptide and against the unmodified peptide. Specificity and selectivity of this antibody was validated by peptide dot blot titrations; Western blots to whole-cell extracts of WT, heterozygous, and homozygous mutant huntingtin cells; immunofluorescence with peptide competition and lack of signal in a huntingtin-knockout mouse model; and embryo fibroblasts by Western blot (13). Huntingtin recruitment to DNA-damage adducts, which was visualized by multiple independent huntingtin monoclonal antibodies, was also demonstrated using this antibody (5). The antibody was also used to define the phospho-dependent switch in huntingtin conformation (32), the increased phosphorylation of huntingtin by ganglioside GM1 treatment of mice (18), and the role of methionine M8 sulfoxidation as a precursor to N17 phosphorylation (11).

The anti–N17-S13pS16p antibody was directly labeled, and direct immunofluorescence was performed on ST$Hdh^{Q7/Q7}$ cells (33) treated with a library of 133 compounds. Images were taken in an unbiased manner with a 40× objective at five software-randomized locations per well with hardware autofocus. There was no investigator observation beyond the first well, where exposure levels were set within the camera dynamic range.

The 12-bit depth images were analyzed by PhenoRipper software (34) in a single channel by assaying image textures. These are a set of pixel-level and space metrics calculated in image processing, designed to quantify the perceived texture of an image. PhenoRipper measures multiple bitmap texture elements in each image, defines the three most variant textures, and uses these three variances to plot a vector in unitless 3D space without any predetermined parameters so that the points farthest from one another represent the most dissimilar images within that dataset. The plot is generated by principal component analysis (PCA) within the dataset and thus has no units on the axes. Hits were chosen based on which compounds plotted furthest from the vehicle control, 0.01% DMSO (Fig. 1*A*). A summary of these of hits, shown in *SI Appendix*, Fig. S1*A*, includes several antiinflammatory, antioxidant, and apoptosis-inducing compounds as well as several compounds that did not fall into any specific category (summarized in Fig. 1*B*).

Antioxidant compounds plotted distinctly from vehicle control, as is consistent with our previous study, which defined methionine M8 sulfoxidation as a trigger of S13/S16 phosphorylation by affecting N17 helicity (11). Another distinct group of compounds was annotated as antiinflammatories. This is consistent with our results from another previous study implicating the IKKβ pathway in regulating huntingtin phosphorylation (13), which has been previously defined by Thompson et al. (30) as the trigger for huntingtin degradation. One of the most distant hit compounds from the control that did not plot near any antiinflammatories or antioxidants had the most effect in the system: N6FFA (Fig. 1*C*). N6FFA is a BBB-permeable compound (31, 35) with a potent effect on the phospho-N17 signal. We therefore selected N6FFA for further investigation.

N6FFA Increases Phosphorylation of N17 in Cells Expressing Mutant Huntingtin and Is Protective in Cell Models of HD. To further understand the effects of N6FFA, we directly examined the phosphorylation state of N17 by immunoblot in mouse striatal-derived cells expressing either WT or humanized mutant huntingtin [ST$Hdh^{Q7/Q7}$ and ST$Hdh^{Q111/Q111}$, respectively (33)] with increasing doses of N6FFA. In WT cells treated with N6FFA, we observed a modest increase in N17 phosphorylation that did not reach significance (Fig. 1*D*). This modest increase was amplified by the more sensitive immunofluorescence technique used in the initial screen in which N6FFA was identified as a hit. In contrast, when we tested the effect of N6FFA on HD-knockin homozygote model cells expressing expanded huntingtin (ST$Hdh^{Q111/Q111}$), we observed a robust and statistically significant increase in N17 phosphorylation (Fig. 1*E*). The optimal treatment concentration was between 0.5–1 μM for a time of 24 h. These results validated N6FFA as a hit from the high-content analysis screen and a modulator of N17 phosphorylation.

As phosphorylation of mutant huntingtin is a protective modification (16, 18), we next asked whether N6FFA affected cell viability. We found that N6FFA was protective in ST$Hdh^{Q111/Q111}$ cells against serum starvation-induced stress, with a significant reduction in annexin V staining noted at a concentration of 10 μM, as shown in *SI Appendix*, Fig. S1*B*. This effect was not seen in ST$Hdh^{Q7/Q7}$ cells. Previous studies have reported substantially different thresholds for N6FFA cytotoxicity, with some groups reporting decreased cell viability at doses as low as 500 nM (36) and others seeing a decrease in viability at doses as high as 100 μM (37). As this difference in N6FFA toxicity threshold may be due to cell-type differences, we sought to test the protective effects of this compound against mutant huntingtin-induced toxicity in a more disease-relevant cell type: mouse primary cortical neurons. We transfected mouse embryonic cortical neurons with a fragment of huntingtin (amino acids 1–586) containing either a WT polyglutamine length of 22 aa (N586-HttQ22) or a mutant polyglutamine length of 82 aa (N586-HttQ82) to assay cell death (38) and treated these cells with increasing concentrations of N6FFA. There was a significant protective effect in cells expressing polyglutamine-expanded huntingtin at 1 μM and 10 μM N6FFA (Fig. 1*F*), consistent with the dose–response curves assaying mutant huntingtin phosphorylation in mouse striatal-derived cells (Fig. 1*E*). We saw no significant effect of N6FFA in the neurons expressing WT huntingtin at any of the concentrations tested (Fig. 1*F*).

Thus, we have identified N6FFA as a compound that affects N17 phosphorylation and promotes cell viability in a dose-dependent manner in mutant huntingtin-expressing cells.

N6FFA Treatment Reduces Cortical Mutant Huntingtin Inclusions and Improves Phenotypes in an HD Mouse Model. Having determined that N6FFA was protective in an HD neuronal model, we next tested the effect of N6FFA on the motor phenotypes of the YAC128 HD mouse model (39). This is a transgenic mouse model

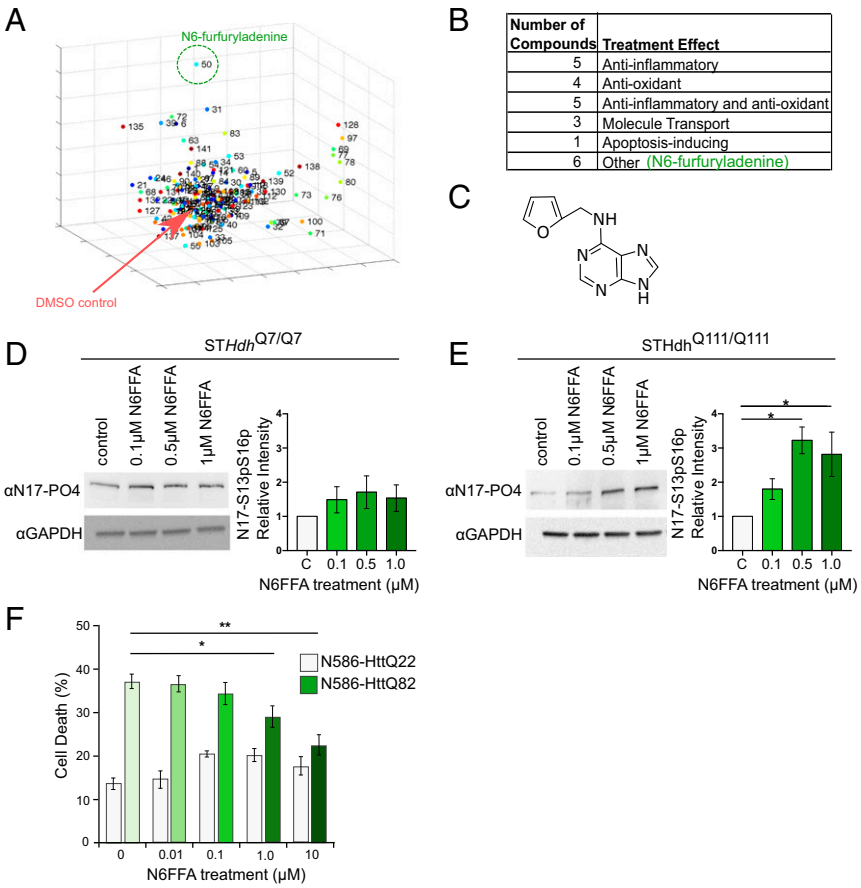

Fig. 1. Identification and validation of N6FFA as a modulator of N17 phosphorylation. Cells were methanol fixed and stained with a primary conjugate antibody recognizing N17 with phospho-groups at S13 and S16 (N17-S13pS16p). Five images per well were taken with a 40× air objective. Images were analyzed by PhenoRipper open source software. A unitless PCA plot and a summary of hits are presented in *A* and *B*, respectively. Compound 134, indicated by a red arrow, represents vehicle control; compound 50, encircled in green, represents N6FFA. (*C*) Chemical structure of N6FFA. (*D* and *E*) STHdh$^{Q7/Q7}$ (*D*) and STHdh$^{Q111/Q111}$ (*E*) cells were treated with the indicated concentrations of N6FFA for 24 h, and total cell lysates were separated by SDS/PAGE followed by immunoblotting with N17-S13pS16p antibody. Pixel intensity results from three independent replicates were quantified. Asterisks indicate concentrations of N6FFA that significantly increased N17 phosphorylation compared with control as determined by an unpaired two-tailed *t* test (*$P < 0.05$). Bars represent mean values ± SEM. (*F*) Mouse cortical neurons were transfected with N586-HttQ22 or N586-HttQ82 and were treated with various concentrations of N6FFA. A nuclear condensation assay was performed to determine percent of cell death. Asterisks indicate concentrations of N6FFA that significantly decreased cell death as determined by an unpaired two-tailed *t* test from three independent replicates (*$P < 0.05$; **$P < 0.001$).

in which a full-length copy of human huntingtin bearing 128 CAG repeats is expressed on a yeast artificial chromosome (YAC). Mice were i.p. injected with N6FFA daily at ∼8 mo of age. As this modality is highly stressful, with mice being handled and receiving painful injections regularly, all mice lost body weight during the course of the treatment (*SI Appendix*, Fig. S2*A*). Motor tests, but not anxiety tests, were therefore pursued in this experiment. While YAC128 mice performed significantly worse than WT littermates on both the accelerating and fixed rotarod motor coordination assays as determined by two-way ANOVA, YAC128 mice that received i.p. injection of N6FFA exhibited increased latency to fall for both tests (accelerating rotarod: effect of genotype, $F_{1,26} = 11.86$, $P = 0.002$; effect of treatment, $F_{2,26} = 4.974$, $P = 0.015$; fixed rotarod: effect of genotype, $F_{1,26} = 5.542$, $P = 0.026$; effect of treatment, $F_{2,26} = 11.94$, $P = 0.0002$) (Fig. 2 *A* and *B*). The motor behavior of YAC128 mice, as measured by the narrow beam test, was also improved with N6FFA treatment (Fig. 2*C*). There was also some improvement in motor phenotypes in WT control mice upon N6FFA dosing. This is consistent with the effects of N6FFA on WT huntingtin phosphorylation (Fig. 1*C*) and with the primary screen assaying WT huntingtin (Fig. 1*A*).

To observe the effects of N6FFA in a modality that was less stressful, allowing acquisition of more reliable data related to anxiety-like behavior, as well as being more amenable to patient treatment, we dosed the animals orally at ∼9 mo of age with N6FFA added to chow for 49 d. At this lower dose and oral modality, no motor-correction effects were noted. We then assessed the effect of N6FFA oral dosing on YAC128 anxiety phenotypes, given that this modality did not inflict a pain stress on the mice. While YAC128 mice spent more time in the closed arms of the elevated plus maze than WT mice (effect of genotype, $F_{1,30} = 5.670$, $P = 0.02$), indicating increased anxiety, N6FFA treatment did not correct this behavior (Fig. 2*D*). On the other hand, N6FFA decreased anxiety behavior and restored exploratory activity in the first 5 min of the open field arena test (effect of treatment, $F_{1,33} = 11.26$, $P = 0.002$) (Fig. 2*E*). We next measured fecal boli dropped in conditions that elicit anxiety. In the forced swim test, YAC128 mice released more fecal pellets than WT littermates, an indication of increased anxiety that was reversed by the administration of N6FFA (effect of genotype, $F_{1,34} = 5.773$, $P = 0.02$; effect of treatment, $F_{1,34} = 3.896$, $P = 0.05$) (Fig. 2*F*). In summary, N6FFA improved YAC128 motor phenotypes by i.p. administration, and anxiety-like phenotypes by oral administration.

We next asked whether the effect of N6FFA on YAC128 phenotypes is due to a direct effect on the huntingtin protein. We measured the levels of insoluble mutant huntingtin inclusions in

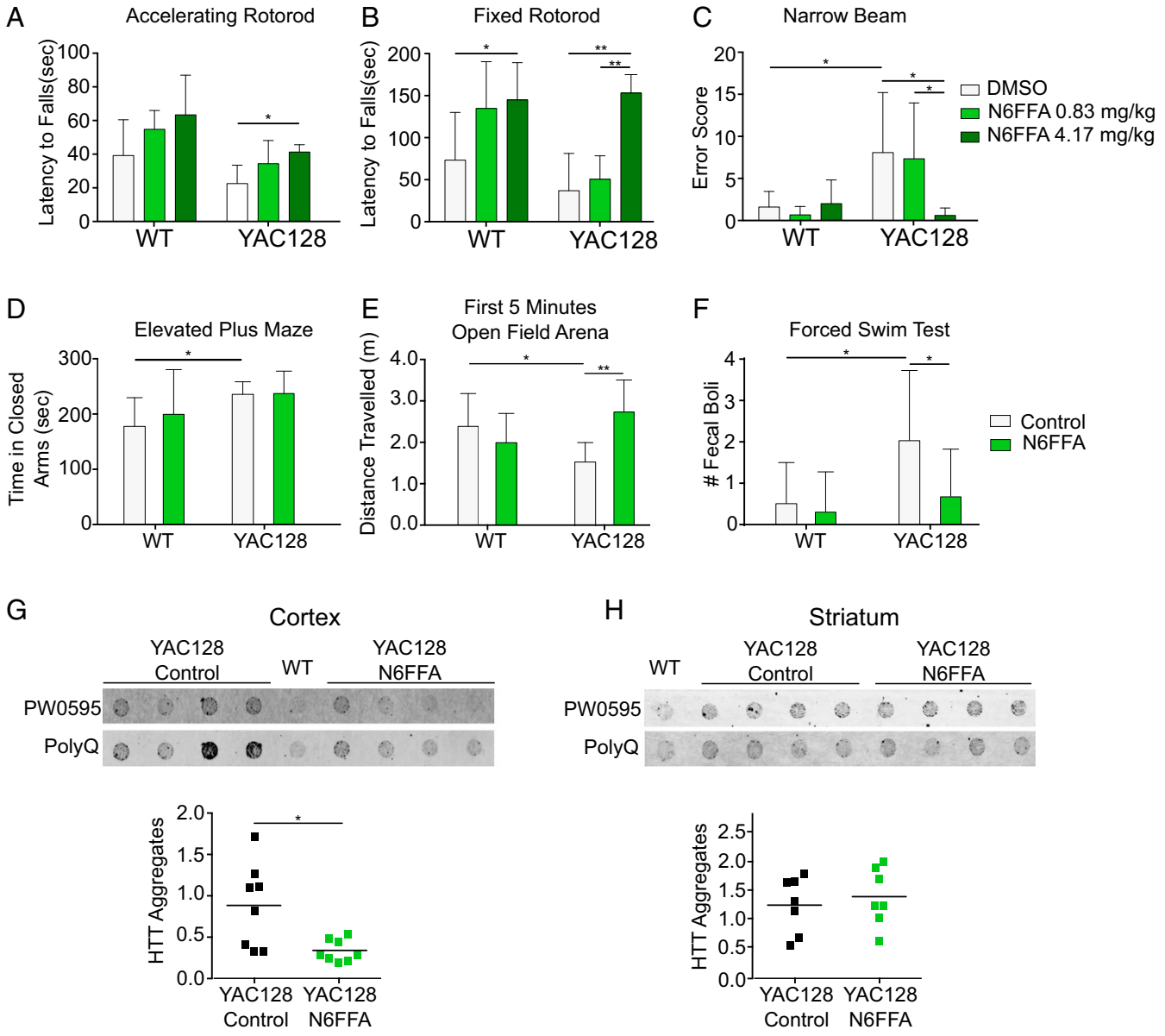

Fig. 2. Effects of N6FFA administration on motor performance, anxiety-like behavior, and huntingtin inclusions in YAC128 mice. (*A*) Mice were tested on an accelerating rotarod (4–40 rpm in 2 min) after 42 d of daily i.p. injection of N6FFA or vehicle (1.5% DMSO). (*B*) Mice were tested on a fixed-rate rotarod (12 rpm) after 42 d of i.p. injection of N6FFA or vehicle. In *A* and *B* $n = 7$ for WT DMSO, and $n = 5$ for WT N6FFA (0.83 mg/kg and 4.17 mg/kg), YAC128 DMSO, and YAC128 N6FFA (0.83 mg/kg and 4.17 mg/kg). (*C*) Mice were tested in the narrow beam test. $n = 6$ for WT DMSO, WT N6FFA 4.17 mg/kg, and YAC128 N6FFA 4.17 mg/kg; $n = 5$ for WT N6FFA 0.83 mg/kg, YAC128 DMSO, and YAC128 N6FFA 0.83 mg/kg. (*D*) Time in the closed arms of the elevated plus maze was tested. $n = 10$ for WT control and for WT N6FFA; $n = 7$ for YAC128 control and for YAC128 N6FFA. (*E*) Exploratory activity in the first 5 min spent in an open field arena is shown. $n = 10$ for WT control and for WT N6FFA, $n = 8$ for YAC128 control, and $n = 9$ for YAC128 N6FFA. (*F*) The number of fecal pellets released in the forced swim test was measured. $n = 10$ for WT control and for WT N6FFA; $n = 9$ for YAC128 control and for YAC128 N6FFA. (*G* and *H*) SDS-insoluble aggregates of mutant huntingtin were measured in YAC128 cortex (*G*) or striatum (*H*) after treatment with control or N6FFA-containing diet ($n = 8$ for YAC128 control diet; $n = 7$–9 YAC128 N6FFA diet). Representative membranes and pixel intensity analysis are shown ($^*P < 0.05$). Statistical analysis was performed using two-way ANOVA and Bonferroni posttest for mouse performance and Student's *t* test for insoluble mutant huntingtin data. In all panels, error bars represent mean ± SEM.

the brains of control-treated and N6FFA-treated YAC128 mice. As shown in Fig. 2*G*, upon N6FFA treatment the levels of insoluble mutant huntingtin protein were dramatically decreased in the cortex but not in the striatum (Fig. 2*H*). While we hypothesize that this difference may be due to incomplete delivery of N6FFA to the striatum, with most of the compound metabolized in the cortex, as directed by cerebrospinal fluid flow, we have not investigated this phenomenon further. We also investigated levels of insoluble mutant huntingtin in the striatum and cortex of the mice that received i.p. injections of N6FFA. In the cortex, we again see significantly decreased levels of insoluble huntingtin; in the striatum, a trend toward decreased levels of insoluble mutant huntingtin did not reach significance (*SI Appendix*, Fig. S2 *B* and *C*). Thus, we observed protective effects of N6FFA in HD cell and mouse models, with direct effects on huntingtin protein levels.

The Metabolic Product of N6FFA/Kinetin, KTP, Can Be Used as a Phospho-Donor by CK2 to Phosphorylate N17. We next evaluated possible mechanisms of N6FFA action. Cells can metabolize exogenously applied N6FFA/kinetin to KTP by means of the

nucleotide-salvaging enzyme APRT (25). The resulting ATP analog, KTP (*SI Appendix*, Fig. S3*A*), can be used by PTEN-induced putative kinase 1 (PINK1) for the transfer of its gamma-phosphoryl group to the PINK1 substrate (25). The kinase CK2 can utilize multiple substrates as phospho-donors, including GTP and ATP (40). We have previously reported that CK2 is a putative N17 kinase, based on results of a kinase inhibitor screen with multiple CK2 inhibitors as hits (13). More precise effects were achieved by treatment with nanomolar levels of the CK2 inhibitor DMAT (41), with inhibition of CK2 specifically decreasing phosphorylation of N17 (13). We therefore hypothesized that the mechanism by which N6FFA increases N17 phosphorylation is through its metabolism to KTP and use by CK2 as a phospho-donor for huntingtin N17.

To test whether CK2 can use KTP to phosphorylate its canonical substrates, we performed a peptide array assay comparing CK2 kinase activity with either ATP or KTP as phospho-donors. A full table of these peptides is presented in *SI Appendix*, Fig. S3. As shown in *SI Appendix*, Fig. S3*B*, CK2 phosphorylates numerous substrates to similar degrees using either ATP or KTP.

We next asked whether CK2 can directly phosphorylate the N17 domain in vitro. We found that CK2 can use either ATP or KTP to phosphorylate N17, provided that S13 is already primed by phosphorylation (Fig. 3 *A* and *B*). This is consistent with the description of CK2 as a ubiquitous acidophilic kinase, where its activity is typically regulated by the substrate and priming adds a negative charge to the site (42). To confirm that the effect we are seeing is mediated by CK2, we treated cells with N6FFA in the presence of DMAT (41). DMAT prevented N6FFA from modulating N17 phosphorylation levels (Fig. 3*C*), consistent with previous work that defined CK2 as a N17 kinase (13). Thus, the restoration of N17 phosphorylation by N6FFA can be blocked by the inhibition of CK2.

To form KTP for utilization by CK2, N6FFA must be salvaged to the triphosphate form. To test if N6FFA salvaging to KTP is critical for the observed increase in N17 phosphorylation, we treated cells with 9-diaza-kinetin (9DK), a derivative of N6FFA that cannot be salvaged due to a nonhydrolysable nitrogen–nitrogen diaza-bond at nitrogen nine (structures are shown in Fig. 3*D*). In contrast to N6FFA, 9DK did not cause an increase in huntingtin phosphorylation in ST*Hdh*$^{Q111/Q111}$ cells (Fig. 3*D*), indicating that the increase in N17 phosphorylation upon N6FFA treatment occurs through its conversion to KTP by nucleotide salvaging.

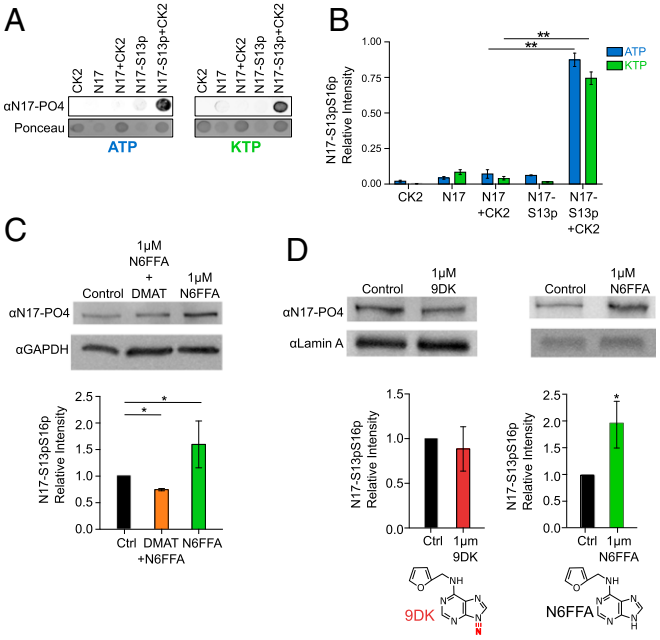

Fig. 3. CK2 uses KTP as a phospho-donor to phosphorylate huntingtin N17 when primed by phosphorylation. (*A* and *B*) Representative blot (*A*) and quantification (*B*) of an in vitro N17 phosphorylation assay using CK2 with either ATP or KTP as phospho-donor. $^{**}P < 0.001$, Mann–Whitney test; $n = 3$ independent replicates. (*C*) Representative blot (*Upper*) and quantification (*Lower*) of N17-S13pS16p levels in STHdh$^{Q111/Q111}$ cells upon treatment with N6FFA with or without the addition of the CK2 inhibitor DMAT (4.5 μM). $^{*}P < 0.05$, Mann–Whitney test ($n = 4$ independent replicates). (*D*) Representative blot (*Upper*) and quantification (*Lower*) of N17-S13pS16p levels in STHdh$^{Q111/Q111}$ cells upon treatment with the nonhydrolysable N6FFA derivative 9DK (analysis by Mann–Whitney test) (*Left*) or treatment with N6FFA (analysis by unpaired t test) (*Right*). $n = 3$ independent replicates for both experiments; $^{*}P < 0.05$. For all data, error bars show mean ± SEM.

Components of the N6FFA Salvaging and Signaling Pathway Functionally Colocalize at Sites of DNA Damage. CK2 is a constitutively active kinase regulated, in part, by subcellular localization and proximity to its substrates (43). CK2 is well characterized to phosphorylate DNA-repair factors (44), and we previously defined huntingtin at sites of ATM-mediated DNA repair (5). We therefore asked whether CK2 and huntingtin colocalize within the cell both at resting states and during active DNA-damage repair. We have previously reported that the anti–N17-S13pS16p antibody highlights insoluble, chromatin-dependent nuclear puncta (5, 11, 13), which we recently identified as nuclear speckles (19). Using antibodies against CK2 and N17-S13pS16p and superresolution structured illumination microscopy (SR-SIM), we observed colocalization of these endogenous proteins at nuclear speckles (Fig. 4*A*), suggesting that CK2 kinase activity on N17 may take place in the nucleus, similar to CK2 activity on DNA-repair proteins (45) such as XRCC1 (46) or P53BP1 (47).

N6FFA is an endogenous byproduct of oxidative DNA damage, whereby the addition of a furfuryl group to an adenosine base within the DNA backbone under Fenton reaction-oxidizing conditions generates N6FFA riboside (23). The generation of this adduct is followed by excision of N6FFA from the DNA backbone (48). We have shown that the huntingtin protein acts as a scaffold for DNA-repair proteins in response to oxidative stress (5). The importance of this role was given context when the results of a large GWAS study revealed a high number of DNA-repair genes as modifiers of age of disease onset (3). Similar to the protective effects we observed in HD model mice (Fig. 2), a recent study showed neuroprotective effects of N6FFA against radiation-induced behavioral changes in a Swiss albino mouse model (49). Together, these findings prompted us to investigate a connection between N6FFA and huntingtin in the context of DNA damage.

We first asked whether we could directly detect N6FFA riboside and the nucleotide-salvaging protein APRT at sites of DNA damage where huntingtin is known to accumulate (5). Using a 405-nm laser, we induced DNA damage in a line across chromatin. After 20-min incubation, endogenous CK2 and huntingtin phosphorylated at N17 were enriched at the irradiated regions of DNA damage (Fig. 4*B*). Unlike steady-state imaging at nuclear puncta, this functional relocalization with colocalization was triggered by induced DNA damage. While protein colocalization alone is not definitive of interactions, the functional colocalization of these proteins supports the concept that they are functioning as part of a complex relevant to functions in DNA-damage repair. Furthermore, both the oxidative DNA-damage product, N6FFA riboside (Fig. 4*C*), and the salvaging enzyme responsible for converting this product to KTP, APRT (25) (Fig. 4*D*), concentrated at the same DNA-damage sites. Thus, components of the N6FFA salvaging pathway functionally colocalize to sites of DNA damage.

We previously found that huntingtin localization to sites of DNA damage is dependent on ATM kinase activity (5). We therefore asked whether APRT recruitment is regulated in a similar fashion.

CELL BIOLOGY

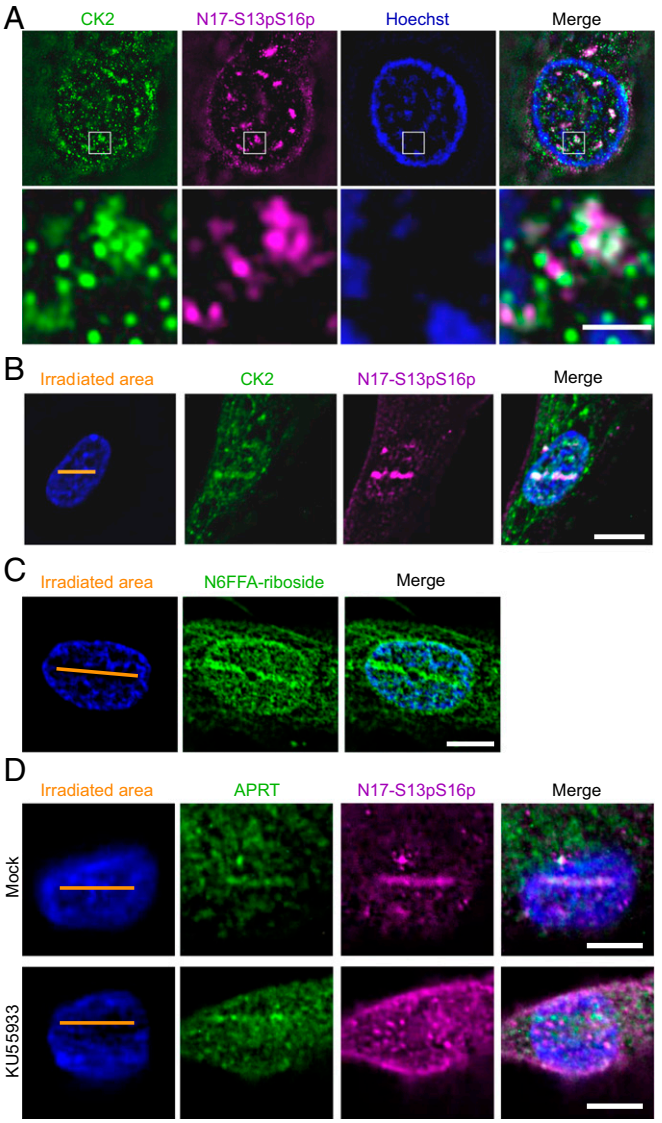

Fig. 4. Components of the N6FFA–APRT–KTP–CK2–huntingtin pathway colocalize at sites of DNA damage. (*A*, *Upper*) Human fibroblasts were stained with anti-CK2 (green) and anti–N17-S13pS16p (magenta) and were imaged using SR-SIM. (*Lower*) Magnified views of the boxed areas. (Scale bar: 1 μm.) (*B*) Human fibroblasts were irradiated with a 405-nm laser in the indicated region to induce DNA damage. After a 20-min incubation period, immunofluorescence was performed against CK2 (green) and N17-S13pS16p (magenta), and the x and y coordinates were revisited to image the irradiated cells by Z-stacked wide-field microscopy and deconvolution. We observed a 100% correlation between CK2 and N17-S13pS16p localization to irradiated regions in two experiments (n = 20–30 cells per experiment). (*C*) Human fibroblasts were irradiated as in *B*, stained with anti-N6FFA riboside (green), and imaged by Z-stacked wide-field microscopy and deconvolution. (*D*) Human fibroblasts were treated with vehicle control (mock) or 10 μM KU55933 for 25 min and then were irradiated as in *B*, stained with anti-APRT (green) and anti–N17-S13pS16p (magenta), and imaged by Z-stacked wide-field microscopy and deconvolution. (Scale bars: 10 μm in *B*–*D*.)

As shown in Fig. 4*D*, APRT could still localize to UV irradiation sites in the presence of the ATM inhibitor KU55933 (50) under conditions that inhibit huntingtin recruitment. This suggests that recruitment of the nucleotide salvager APRT to DNA-damage sites and KTP generation do not require ATM activation, and hence do not require huntingtin recruitment. CK2 is required for P53BP1 accumulation at sites of DNA damage, which is a prerequisite for efficient activation of the ATM-mediated signaling pathway (47). Huntingtin makes up part of the ATM complex, and its recruitment to DNA damage is blocked by ATM kinase inhibition (5). These results allow us to hypothesize a mechanism in which KTP, produced proximal to DNA damage via APRT activity, is used by CK2 to phosphorylate substrates in the ATM DNA damage-repair response, including the huntingtin N17 domain. Thus, this salvaged product of oxidative DNA damage may act as a signaling molecule to potentiate DNA repair (Fig. 5) under the repair-associated conditions of a low-ATP "energy crisis" (29).

Discussion

Many current drug-discovery efforts are limited to high-throughput analysis with low-resolution endpoints (51). As an alternative, we used high-content analysis to screen a small library of natural compounds encompassing a wide breadth of biologically active chemical space to define modulators of N17 phosphorylation. We show that high-content analysis of endogenous phosphorylated huntingtin is extremely effective for identifying potential disease-modifying compounds. The use of PCA and image textures allowed us to visualize the degree to which compounds affected N17-S13pS16p signal properties without bias, in that we did not predefine any parameters for sorting. We found that the two predominant types of compounds affecting our assay were antiinflammatory agents and antioxidants. Consistent with this finding, we and others have previously shown that inhibition of IKKβ within the NF-κB inflammation pathway affects huntingtin phosphorylation (13, 30).

The identification of antioxidants as modulators of N17 phosphorylation is also compelling, given the implication of ROS in HD pathology (52). The antioxidant XJB-5-131 is known to modify toxicity in an HD model, by either preventing onset or improving pathophysiology in a mouse that has developed disease (53). Our group has recently shown that huntingtin acts as an ROS sensor, elucidating a mechanism by which sulfoxidation of methionine eight within N17 leads to increased huntingtin solubility from lipid membranes of the ER, enhancing S13/S16 phosphorylation and translocation of huntingtin to the nucleus (11). The identification of several antioxidant compounds in our screen supports these findings, as these compounds reduced the phospho-N17 signal. In the context of ROS, increased N17 phosphorylation upon IKKβ inhibition may be due to the prevention of the NF-κB pathway ROS signaling response and the resulting elevated intracellular ROS levels (54).

The N6FFA compound was selected for further experimentation as it has been demonstrated in animal models to be both BBB permeable (31) and neuroprotective (49). We show a protective effect of N6FFA in a cell line expressing a severe toxic

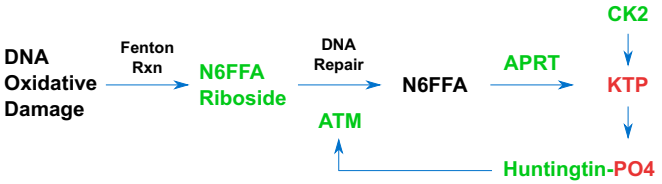

Fig. 5. A product of oxidative DNA repair is used by CK2 to phosphorylate huntingtin at sites of DNA damage. DNA is oxidized via the Fenton reaction by age-onset reactive oxygen stress. N6-furfuryladenine riboside results and is excised by the DNA damage-repair machinery. APRT salvages the excision product, N6FFA, to yield KTP. KTP is used as a phosphate donor by CK2 to modify huntingtin N17, and potentially other DNA-repair proteins, in a positive-feedback mechanism. We hypothesize that exogenous administration of N6FFA potentiates the reaction. All components of the model seen to functionally colocalize proximal to DNA-damage regions are highlighted in green.

mutant huntingtin fragment in cortical neuronal culture. This is consistent with other studies showing protective effects of N6FFA under conditions of stress (22, 36, 49, 55, 56). N6FFA has been broadly categorized as an antioxidant (21); however, we note that N6FFA increases huntingtin phosphorylation, whereas antioxidants decrease phosphorylation (11). More recent studies have shown that N6FFA is not effective in scavenging free radicals (55) but instead activates other antioxidant defense mechanisms (36, 37, 55, 56). Our results support an alternative mechanism in which huntingtin is directly modified by N6FFA.

We observed reduced cortical mutant huntingtin aggregate load upon N6FFA treatment in YAC128 mice. Previous findings have shown that mutant huntingtin is not properly degraded, leading to toxic accumulation (57). Studies have shown that phosphorylation of huntingtin mediates clearance (30, 58, 59) and that mutant huntingtin is hypophosphorylated at many sites of proteolytic activity (60). Huntingtin N17 phosphorylation enhances protein clearance by the proteasome and lysosome (30). Our results are consistent with increased mutant huntingtin phosphorylation, via administration of N6FFA, mediating protein clearance. With the efficacy of N6FFA established, we next sought to determine the mechanism.

The report that the metabolic product of N6FFA, KTP, is an ATP analog that can be utilized by PINK1 as a phospho-donor (25) prompted us to investigate a similar mechanism for CK2, which we previously identified as a regulator of N17 phosphorylation (13). CK2 exhibits unusual catalytic-site flexibility and is one of the few known kinases that can use both ATP and GTP as phosphate donors (42). We found that CK2 can also use KTP to phosphorylate its substrates, including N17. Furthermore, N17 phosphorylation was not achieved with a nonhydrolyzable N6FFA derivative or in the presence of a CK2 inhibitor, implicating nucleotide-salvaging activity and CK2 activity as crucial elements of the N6FFA effect. As KTP is also used by PINK1 to regulate mitochondrial proteostasis, and enhanced mitochondrial proteostasis is protective against β-amyloid proteotoxicity (61), some pleiotropy of KTP-mediated signaling could be beneficial beyond just phospho-huntingtin correction.

We found that CK2 colocalizes with N17-phosphorylated huntingtin at nuclear speckles. CK2 is a ubiquitous kinase known to modify proteins involved in DNA repair (46, 62), and huntingtin is part of the ATM oxidative DNA damage-response complex (5). The influence of DNA-repair pathways on HD disease onset, revealed by GWAS (3, 4, 63), suggests that ROS and DNA-damage repair are critical modifiers for HD age of onset. CK2 may be phosphorylating huntingtin N17 at these nuclear puncta in response to oxidative DNA damage. This is similar to the way CK2 phosphorylates the deubiquitinating enzyme OTUB1, mediating its nuclear entry and the formation of P53BP1 DNA-repair foci (64).

N6FFA riboside is a known product of oxidative DNA damage via the Fenton reaction, causing perturbation of the DNA structure (48, 65). Upon induction of DNA damage via 405-nm laser, we detected N6FFA riboside generated within the DNA. We propose that, following excision from the DNA, N6FFA is salvaged to KTP via the mechanism proposed by Hertz et al. (25). The accumulation of huntingtin, CK2, N6FFA, and the nucleotide salvager APRT at DNA-damage sites suggests that the effective local concentration of these pathway factors in proximity to DNA damage facilitates phosphorylation of N17.

In HD, KTP-mediated signaling immediately proximal to DNA damage may be important in the context of low ATP. Aging cells demonstrate significantly decreased ATP levels (66), a condition that is exacerbated in HD (26, 67). The role of huntingtin as a stress-response protein (11, 13, 68) also suggests that a signaling pathway utilizing an alternate source of phosphates may be critical under stress conditions, where most ATP is utilized at the ER lumen for the unfolded protein response (69), which is chronically active in HD (70). The energy deficits seen classically in HD may also be the result of chronic DNA-damage repair, triggered by age-onset ROS stress: The first step of DNA single-strand break damage repair is identification of the lesion by the poly (ADP ribose) polymerase proteins, or PARPs. PARP hyperactivation during DNA damage can result in a cellular energy crisis in which poly (ADP ribose) inhibits ATP production (29). Finally, salvaged purines may be the only potential source of triphosphate in proximity to DNA-damage complexes. Neurons rely heavily on the salvaging rather than de novo synthesis of nucleotides (27, 28), and a recent GWAS identified RRM2B/P53R2, a ribonucleotide-salvaging enzyme, as a modifier of HD age of onset. This highlights a potential important role of salvage pathways in HD (3).

The large number of neurodegenerative disorders for which a DNA-repair protein is defective, suggests that DNA repair may be a critical node for neuronal health, particularly at the ATM complex (71). Given the role of huntingtin as a scaffold for the ATM complex (5), dominant mutant huntingtin effects coupled with an age-related ROS increase could lead to the age-onset accumulation of DNA damage. As mutant huntingtin is hypophosphorylated at the N17 domain (13, 19), and phosphorylation is beneficial in HD models (12, 18), the effects we observed with N6FFA treatment connect DNA-damage repair, altered bioenergetics, and mutant huntingtin phosphorylation and inclusion load.

Materials and Methods

Reagents and Antibodies. All reagents were from Sigma-Aldrich unless otherwise stated. Polyclonal antibody against huntingtin phosphorylated at S13 and S16 of the N17 domain (anti–N17-S13pS16p) was previously characterized and validated (13). To directly conjugate the anti–N17-S13pS16p antibody to Alexa Fluor 488 succinimidyl ester dye (Molecular Probes/Life Technologies), 1 μL dye/10 μL antibody and 5% $NaHCO_3$ were incubated overnight at 4 °C with rotation. The conjugate antibody was then run through a Sephadex G-25 bead (Amersham Pharmacia Biotech AB) column and collected by elution with PBS until the visible dye front reached the base of the column. Additional antibodies used in this study were anti–N17-S13pS16p (New England Peptides), anti-CK2 alpha (Abcam), and anti-N6FFA/kinetin riboside (Agrisera) for immunofluorescence and anti-thiophosphate ester (Abcam), anti-GAPDH (Abcam), rabbit anti-huntingtin (PW0595; Enzo Life Sciences), and mouse anti-polyglutamine (mAB1574, Chand mouse anti-huntingtin) for Western blots. Secondary antibodies against rabbit, mouse, and goat IgG, conjugated to Alexa Fluor 488, 555, 594, or Cy5, were from Invitrogen. Secondary HRP conjugates were from Abcam. Goat anti-rabbit IRDye 800CW, goat anti-rabbit IRDye 680CW, and goat anti-mouse IRDye 800 were from LI-COR Biosciences.

Cells. Cells derived from mouse striatum, ST$Hdh^{Q7/Q7}$ and ST$Hdh^{Q111/Q111}$ (a kind gift from Marcy E. Macdonald, Massachusetts General Hospital/Harvard Medical School), were grown in DMEM with 10% FBS at 33 °C in a 5% CO_2 incubator. Human *hTERT*-immortalized foreskin fibroblast BJ-5ta cells (ATCC) and primary human fibroblasts from Coriell Institute for Medical Research Biorepositories (ND30014 WT fibroblasts bearing 21/18 CAG repeats in *HTT* gene alleles) were grown in minimal Eagle's medium with 15% FBS and 1% Glutamax at 37 °C with 5% CO_2. All media and supplements were from Gibco Life Technologies. Primary cortical neurons were prepared from CD1 mice as described (38). In brief, cortices of E15 DC1 embryos were dissected, quickly dissociated, and plated at 1.10^5 cells/mm^2. Cells were kept in Neurobasal medium supplemented with B27 and 2 mM GlutaMAX (Gibco) in 5% CO_2 at 37 °C throughout the experiment.

High-Content Screen and Analysis. ST$Hdh^{Q7/Q7}$ cells were seeded into 96-well ibiTreat dishes (Ibidi) and grown for 24 h before treatment with a 133-compound natural-compound library (Selleckchem) for 6 h at 33 °C. Immunofluorescence was performed as described below with Alexa Fluor 488-conjugated anti–N17-S13pS16p antibody at 1:15 dilution. Images taken with a 40× objective were analyzed using PhenoRipper (34) in which five images per well were thresholded by random sampling and analysis was carried out using a block size of 15. Hits were scored by selecting the points on the resulting PCA plot lying furthest from controls (outside an arbitrarily defined radius).

Compound Administration to Cells. All compounds were administered in DMEM with 0.2% FBS for 24 h unless otherwise indicated.

Protein Extraction and Immunoblotting. Cells were lysed in either Nonidet P-40 lysis buffer [50 mM Tris·HCl (pH 8.0), 150 mM NaCl, 1% Nonidet P-40] or radioimmunoassay lysis buffer [50 mM Tris·HCl (pH 8.0), 150 mM NaCl, 1% Nonidet P-40, 0.25% sodium deoxycholate, 1 mM EDTA] containing protease and phosphatase inhibitors (Roche). Lysates were centrifuged at 17,000 × *g* for 12 min, and the supernatant was collected for immunoblot analysis. Equal amounts of protein were separated by SDS/PAGE on precast 4–20% polyacrylamide gradient gels (Bio-Rad) and were electroblotted onto Immobilon PVDF membrane (EMD Millipore). Membranes were blocked in Tris-buffered saline with Tween 20 (TBST) [50 mM Tris·HCl (pH 7.5), 150 mM NaCl, 0.1% Tween-20] containing 5% nonfat dry milk for 1.5 h at room temperature, followed by overnight incubation with primary antibodies diluted in blocking buffer (anti–N17-S13pS16p 1:2,500; anti-GAPDH 1:7,500) at 4 °C. After three 15-min TBST washes, membranes were incubated with HRP-conjugated secondary antibodies diluted in blocking buffer (1:50,000) for 45 min at room temperature and were visualized using Immobilon enhanced chemiluminesence HRP substrate (EMD Millipore) on a MicroChemi system (DNR Bio-imaging Systems). Bands were quantified using NIH ImageJ software and were normalized to GAPDH controls.

In Vitro Kinase Assays. GST-CK2α was purified from bacterial culture as previously described (72). Enzyme concentration was determined by absorbance at 595 nm, measured on a Victor3 V 1420 multilabel counter (Perkin-Elmer) using BSA standards. The enzyme was diluted (up to 1:5,000) in CK2 dilution buffer [5 μM Mops (pH 7.0), 200 mM NaCl, 1 mg/mL BSA] immediately before use in kinase assays.

For the CK2 phospho-donor specificity assay, peptide arrays were synthesized using SPOT technology on nitrocellulose membranes using the AutoSpot Robot ASP 222 (Abimed) as previously described (73, 74). Filters bearing CK2 substrate sequences and controls were moistened with 95% ethanol to ensure solubilization of the peptides on the filter; then an equal volume of water was added with rocking for 15 min. Membranes were washed five times with water and once with kinase assay buffer (KAB) [50 mM Tris·HCl (pH 7.5), 30 mM $MgCl_2$, 50 mM KCl] and were incubated in KAB overnight with gentle rocking. Fresh KAB was added for 1 h at 30 °C with rocking. Then 100 μM ATPγS or KTPγS (Biolog) was added, followed by 100 μM BSA, and the reaction was started by adding CK2α holoenzyme (1:2,500, 32.44 mg/mL with 665.1 nmol·min^{-1}·mg^{-1} specific activity) and was incubated at 30 °C with rocking for 20 min. NaCl (1 M) was added to stop the reaction, and membranes were washed five times with water. To alkylate the thiophosphate, the membranes were incubated in 2.5 mM p-nitrobenzyl mesylate (Abcam) in water for 2 h at room temperature and then were washed five times with water. To decrease background noise, membranes were incubated in stripping solution (4 M Guanidine-HCl, 1% SDS, 0.5% β-mercaptoethanol) for 1 h at 40 °C. Membranes were washed 10 times in water and three times in TBST, blocked in 5% milk in TBST for 1 h at room temperature, incubated with thiophosphate ester primary antibody (1:5,000; Abcam) in 5% milk in TBST overnight at 4 °C, and then were washed three times in TBST. Membranes were then incubated for 45-min at room temperature with IRDye 800CW goat anti-rabbit secondary antibody (1:10,000; LI-COR) in 5% BSA in TBST and were then washed three times in TBST and once in TBS. The LI-COR Odyssey imaging system was used to visualize the array.

For in vitro kinase assays with unphosphorylated and S13p-primed N17 peptide, 1,000 ng peptide (New England Peptides) was incubated in 1:5 KAB with 100 μM adenosine triphosphate (Sigma-Aldrich) or N6FFA/kinetin triphosphate (Biolog) in a 10-μL reaction. The reaction was initiated by the addition of CK2α holoenzyme (1:2,500, 32.44 mg/mL with 665.1 nmol·min^{-1}·mg^{-1} specific activity) and was incubated at 30 °C for 15 min with shaking. In each case, the reaction was stopped by placing it on ice, and 8 μL of the kinase assay mixture was spotted onto nitrocellulose membrane (Pall Life Sciences) in 2-μL dots (×4) and allowed to dry for 30 min. Membranes were washed once in TBST and blocked in 5% nonfat milk in TBST for 1.5 h and then were incubated in anti–N17-S13pS16p (1:2,500) overnight at 4 °C with rocking. Membranes were then washed three times in TBST and were incubated with HRP-conjugated secondary antibody (1:50,000; Abcam) and were visualized using Immobilon enhanced chemiluminesence (EMD Millipore) on a MicroChemi system (DNR Bio-imaging Systems) or were incubated with IRDye 800CW goat anti-rabbit secondary antibody (1:10,000; LI-COR) and were visualized on a LI-COR Odyssey system. The signal intensity of the dots was quantified using ImageJ software.

Immunofluorescence. Cells were grown to ∼80% confluence in 96-well ibi-Treat dishes (Ibidi) for screening or in glass-bottomed tissue-culture dishes for irradiation experiments before the indicated treatments. Fixation and permeabilization by methanol at −20 °C for 10 min was followed by washing with wash buffer [50 mM Tris·HCl (pH 7.5), 150 mM NaCl, 0.1% Triton X-100] and blocking for 1 h at room temperature with blocking buffer (wash buffer + 2% FBS). Cells were incubated with primary antibodies diluted in blocking buffer for either 1 h at room temperature or overnight at 4 °C before washing and imaging in PBS (Alexa Fluor 488-conjugated anti–N17-S13pS16p) or incubation with secondary antibodies diluted in blocking buffer for 30 min at room temperature. After washing, nuclei were stained with Hoechst (0.2 μg/mL in PBS) for 5 min at room temperature, washed, and imaged in PBS. Cells grown for SR-SIM imaging were seeded onto no. 1.5 coverslips, fixed and stained as above, and mounted on glass slides using frame slide chambers (Bio-Rad). Cells stained with the anti-N6FFA antibody were fixed and permeabilized in 1:1 methanol:acetone at −20 °C for 10 min, washed with PBS, then incubated with 2 M HCl for 45 min at room temperature to denature DNA. Following neutralization in 50 mM Tris·HCl (pH 8.8) for 5 min and washing with PBS, cells were blocked and stained as above.

Induction of DNA Damage. For microirradiation experiments, cells were grown overnight in glass-bottomed dishes and then were stained with NucBlue (Molecular Probes/Life Technologies) for 15 min at 37 °C in a 5% CO_2 incubator. The medium was replaced with HBSS (Gibco) immediately before microirradiation. Cells were irradiated using the Nikon C2+ confocal system equipped with an InVivo Scientific environmental chamber held at 37 °C. Regions of interest (∼20 pixels each) were irradiated at a scan speed of 16 s per frame (512 × 512) using a Coherent OBIS 405-nm diode laser (Coherent, Inc.) set to 100% power. The x and y coordinates were recorded, and cells were incubated at 37 °C for the indicated periods before fixation and immunofluorescence. The x and y coordinates were then revisited to image the irradiated cells.

Microscopy. Wide-field epifluorescence microscopy was done on a Nikon Eclipse Ti wide-field epifluorescent inverted microscope using a PLAN FLUOR 40×/0.6 air objective (for screening), or a PLAN apochromat (APO) 60×/1.4 oil objective and Spectra X LED lamp (Lumencor). Images were captured using a Hamamatsu Orca-Flash 4.0 CMOS camera (Hamamatsu). Image acquisition and deconvolution of Z-stacks were done with NIS-Elements Advanced Research version 4.30 64-bit acquisition software (Nikon Instruments). Super-resolution imaging was done on the Nikon N-SIM superresolution microscope system attached to a Nikon Eclipse Ti inverted microscope using an APO total internal reflection fluorescence (TIRF) 100×/1.49 oil objective and 405-nm, 488-nm, and 561-nm lasers (Coherent, Inc.). Images were captured using a Hamamatsu Orca-Flash 4.0 CMOS camera and were acquired with NIS-Elements software version 4.50.

Animal Care and N6FFA Trials. Male YAC128 mice overexpressing the human *HTT* gene with 128 CAG repeats (39) were originally purchased from Jackson Laboratories and subsequently were maintained on an FVB background in the animal facility at the University of Alberta. All mice were maintained on a 12-h/12-h light-dark cycle in a temperature- and humidity-controlled room. All procedures involving animals were approved by the University of Alberta's Animal Care and Use Committee and were in accordance with the guidelines of the Canadian Council on Animal Care. All YAC128 mice and WT littermates used in our studies were males.

Treatment started between 6 and 10 mo of age, and motor testing began 14 d after the start of treatment. For experiments involving i.p. injection, all mice were group housed for the duration of treatment. For experiments involving oral administration, mice were individually housed for the duration of treatment. Animals in all experimental groups were carefully matched for age.

I.p. N6FFA Administration. Mice were 6–9 mo old at the beginning of treatment. N6FFA (0.83 mg/kg or 4.17 mg/kg of body weight, in 1.5% DMSO in saline solution) was administered daily at 1600 h by i.p. injection, alternating the side of injection. Control mice were injected with 1.5% DMSO in saline. Animals in all experimental groups were carefully matched for age (average animal age ± SD: WT saline, 8.1 ± 1.08 mo; WT N6FFA 6 mg/kg, 7.51 ± 1.51 mo; WT N6FFA 30 mg/kg, 7.91 ± 1.31 mo; YAC128 saline, 7.2 ± 1.50 mo; YAC128 6 mg/kg N6FFA, 7.2 ± 1.60 mo; YAC128 30 mg/kg N6FFA, 7.0 ± 1.57 mo).

Oral N6FFA Administration. Mice were 8–10 mo old at the beginning of treatment. A chow diet supplemented with 653 mg N6FFA/kg chow

(OpenSource Diets) was administered for 49 d. Each mouse was provided with 10 g of chow diet, and food was replaced every second day, so that food was available ad libitum. Food intake was measured every second day at 1700 h. Body weight was measured weekly. Animals in all experimental groups were carefully matched for age (average animal age ± SD: WT control chow, 8.9 ± 0.68 mo; WT N6FFA chow, 9.0 ± 0.69 mo; YAC128 control chow, 9.13 ± 0.74 mo; YAC128 N6FFA chow, 9.12 ± 0.69 mo).

Behavioral Tests. Behavioral testing was conducted in the light phase of the light cycle, between 0800 h and 1800 h. In all behavioral training and testing sessions, mice were allowed to acclimate to the testing room for 1 h. All experiments were performed by experimenters who were blind to animal genotype and treatment. All equipment was cleaned with 70% ethanol after each test and before testing the next animal.

For the rotarod, mice were tested in three consecutive 3-min trials, with a 1-min rest between trials, at a fixed rotarod speed (12 rpm). The time spent on the rotarod in each of the three trials was averaged to give the overall latency to fall for each mouse. A similar training protocol was used to test mice on an accelerating rotarod (4–40 rpm in 2 min). For the narrow beam test, mice were placed at the extremity of a 100-cm-long wooden narrow beam (0.75 cm wide, suspended 30 cm above the floor) and were allowed to traverse the beam from one extremity to the other three times. Mouse performance was recorded with a video camera, and footfalls, body balance, and motor coordination were analyzed using an established footfall scoring system (18). For the open field test mice were placed in an open field apparatus (90 × 90 cm) and were filmed during 30-min sessions as they explored the environment. Distance traveled was measured using EthoVision XT tracking software. At the end of each 30-min session in the open field, the number of fecal pellets dropped by each mouse was counted. For the elevated plus maze, mice were placed in the center of the maze facing the open arm and were left to explore freely for 5 min. Arm crosses into and out of open and closed arms, as well as time spent in each arm were recorded with a video camera and scored. An entry was defined as 75% of the body of the mouse, excluding the tail, entering a compartment.

The forced swim test was performed as in ref. 75 to assess anxiety through the number of fecal boli dropped. Mice were placed for 6 min in a 4-L beaker (25 cm tall, 16 cm wide) filled with 2.6 L of water prewarmed to 23–25 °C. After each session, fecal pellets dropped by each mouse were counted.

Tissue Collection and Processing. Mice were killed by cervical dislocation. Brain tissue was flash-frozen in liquid nitrogen and immediately homogenized in ice-cold lysis buffer [20 mM Tris (pH 7.4), 1% Igepal, 1 mM EDTA, 1 mM EGTA, 50 μM MG132, 1× Roche cOmplete protease inhibitor mixture, and 1× Roche PhosStop phosphatase inhibitor mixture] using a Wheaton homogenizer. Tissue lysates were sonicated twice for 10 s each at power 2 using a Sonic Dismembrator Model 100. Protein concentration was measured with the bicinchoninic acid (BCA) assay.

Filter Retardation Assay. The filter retardation assay was performed as described (39, 76), with minor modifications. Briefly, 100 μg of protein lysates were diluted in PBS containing 2% SDS and 100 mM DTT, followed by heating at 100 °C for 10 min. Samples were filtered through a cellulose acetate membrane (0.2-μm pore size; Sterlitech) in a Bio-Dot microfiltration unit (Bio-Rad). Wells were washed twice with PBS. After drying for 30 min, membranes were washed twice with 2% SDS in PBS and then were blocked with 5% BSA in TBST followed by incubation with the primary antibody. IRDye secondary antibodies (LI-COR Biotechnology) were used at 1:10,000 for 1 h at room temperature. The IR signal was acquired and quantified using the Odyssey Imaging System.

Nuclear Condensation Toxicity Assay. The nuclear condensation assay to determine toxicity of the N586 fragment of Htt in neurons was performed as described (38). At 5 d in vitro, neurons were cotransfected with N586-Htt containing either Q22 or Q82 and GFP for 48 h. At the time of transfection, cells were treated with N6FFA doses ranging from 0 to 100 μM. After 48 h, the cells were fixed with paraformaldehyde, and the nuclei were stained with DAPI. Automatic image acquisition was obtained on an Axiovert 200 inverted microscope (Zeiss) using Axiovision. Nuclear staining intensity of GFP^+ cells was quantified automatically using Volocity (Perkin-Elmer). Any cell with an intensity greater than two SDs of the control intensity of untransfected cells was considered dead. Results are presented as a percentage of the total transfected cells.

Annexin V Cell Death Assay. ST$Hdh^{Q7/Q7}$ and ST$Hdh^{Q111/Q111}$ cells were plated in 12-well plates and left to attach overnight. Cells were washed once with Dulbecco's PBS before incubation in serum-free medium (high-glucose DMEM with 400 μg/mL geneticin, 2 mM L-glutamine, and 1 mM sodium pyruvate) containing the indicated concentrations of N6FFA for 9 h at 39 °C. At the end of the incubation period, cells were washed with PBS, trypsinized, washed in PBS, and stained with annexin V PE (BD Pharmingen) in 45 μL of 1× annexin-binding buffer (ABB) (BD Pharmingen) for 15 min at room temperature. Cells were then washed once with 1× ABB and fixed overnight with 2% paraformaldehyde in 1× ABB. FACS analysis of annexin V^+ cells was performed using a CANTO II cell analyzer (BD). Ten thousand events per sample were acquired and analyzed using either CellQuest Pro (BD) or FlowJo analysis software.

Statistical Analysis. For mouse data, all statistical analyses were performed using two-way ANOVA followed by Bonferroni posttest, except for the analysis of body weight, for which repeated-measures two-way ANOVA followed by Bonferroni posttests was used, and for changes in mutant huntingtin expression, for which an unpaired *t* test was performed. All comparisons were performed using a statistical significance level of 0.05. For in vitro and cell-based assays, treatments were compared with control using an unpaired two-tailed *t* test unless data did not pass the Shapiro–Wilk normality test; in that case, Mann–Whitney analysis (two-tailed) was used.

Data and Materials Availability. All reagents and cell lines in this study are available upon request.

ACKNOWLEDGMENTS. This study was supported by Canadian Institutes of Health Research Project Grant MOP-119391, The Krembil Foundation, and the Huntington Society of Canada.

1. MacDonald ME, et al.; The Huntington's Disease Collaborative Research Group (1993) A novel gene containing a trinucleotide repeat that is expanded and unstable on Huntington's disease chromosomes. *Cell* 72:971–983.
2. Keum JW, et al. (2016) The HTT CAG-expansion mutation determines age at death but not disease duration in Huntington disease. *Am J Hum Genet* 98:287–298.
3. Genetic Modifiers of Huntington's Disease (GeM-HD) Consortium (2015) Identification of genetic factors that modify clinical onset of Huntington's disease. *Cell* 162:516–526.
4. Hensman Moss DJ, et al.; TRACK-HD investigators; REGISTRY investigators (2017) Identification of genetic variants associated with Huntington's disease progression: A genome-wide association study. *Lancet Neurol* 16:701–711.
5. Maiuri T, et al. (2017) Huntingtin is a scaffolding protein in the ATM oxidative DNA damage response complex. *Hum Mol Genet* 26:395–406.
6. Zuccato C, Valenza M, Cattaneo E (2010) Molecular mechanisms and potential therapeutical targets in Huntington's disease. *Physiol Rev* 90:905–981.
7. Atwal RS, et al. (2007) Huntingtin has a membrane association signal that can modulate huntingtin aggregation, nuclear entry and toxicity. *Hum Mol Genet* 16: 2600–2615.
8. Godin JD, Humbert S (2011) Mitotic spindle: Focus on the function of huntingtin. *Int J Biochem Cell Biol* 43:852–856.
9. Vidal RL, Hetz C (2012) Crosstalk between the UPR and autophagy pathway contributes to handling cellular stress in neurodegenerative disease. *Autophagy* 8: 970–972.
10. MacDonald ME (2003) Huntingtin: Alive and well and working in middle management. *Sci STKE* 2003:pe48.
11. DiGiovanni LF, Mocle AJ, Xia J, Truant R (2016) Huntingtin N17 domain is a reactive oxygen species sensor regulating huntingtin phosphorylation and localization. *Hum Mol Genet* 25:3937–3945.
12. Gu X, et al. (2009) Serines 13 and 16 are critical determinants of full-length human mutant huntingtin induced disease pathogenesis in HD mice. *Neuron* 64:828–840.
13. Atwal RS, et al. (2011) Kinase inhibitors modulate huntingtin cell localization and toxicity. *Nat Chem Biol* 7:453–460.
14. Michalek M, Salnikov ES, Bechinger B (2013) Structure and topology of the huntingtin 1-17 membrane anchor by a combined solution and solid-state NMR approach. *Biophys J* 105:699–710.
15. Maiuri T, Woloshansky T, Xia J, Truant R (2013) The huntingtin N17 domain is a multifunctional CRM1 and Ran-dependent nuclear and cilial export signal. *Hum Mol Genet* 22:1383–1394.
16. Gu X, et al. (2015) N17 modifies mutant huntingtin nuclear pathogenesis and severity of disease in HD BAC transgenic mice. *Neuron* 85:726–741.
17. Veldman MB, et al. (2015) The N17 domain mitigates nuclear toxicity in a novel zebrafish Huntington's disease model. *Mol Neurodegener* 10:67.
18. Di Pardo A, et al. (2012) Ganglioside GM1 induces phosphorylation of mutant huntingtin and restores normal motor behavior in Huntington disease mice. *Proc Natl Acad Sci USA* 109:3528–3533.
19. Hung CLK, et al. (2018) A patient-derived cellular model for Huntington disease reveals phenotypes at clinically relevant CAG lengths. bioRxiv:10.1101/291575. Preprint, posted March 29, 2018.

20. Barciszewski J, Massino F, Clark BFC (2007) Kinetin–A multiactive molecule. *Int J Biol Macromol* 40:182–192.
21. Olsen A, Siboska GE, Clark BF, Rattan SI (1999) N(6)-Furfuryladenine, kinetin, protects against Fenton reaction-mediated oxidative damage to DNA. *Biochem Biophys Res Commun* 265:499–502.
22. Rattan SIS, Clark BFC (1994) Kinetin delays the onset of ageing characteristics in human fibroblasts. *Biochem Biophys Res Commun* 201:665–672.
23. Barciszewski J, Barciszewska MZ, Siboska G, Rattan SI, Clark BF (1999) Some unusual nucleic acid bases are products of hydroxyl radical oxidation of DNA and RNA. *Mol Biol Rep* 26:231–238.
24. Barciszewski J, Mielcarek M, Stobiecki M, Siboska G, Clark BF (2000) Identification of 6-furfuryladenine (kinetin) in human urine. *Biochem Biophys Res Commun* 279:69–73.
25. Hertz NT, et al. (2013) A neo-substrate that amplifies catalytic activity of Parkinson's-disease-related kinase PINK1. *Cell* 154:737–747.
26. Seong IS, et al. (2005) HD CAG repeat implicates a dominant property of huntingtin in mitochondrial energy metabolism. *Hum Mol Genet* 14:2871–2880.
27. Arnér ES, Eriksson S (1995) Mammalian deoxyribonucleoside kinases. *Pharmacol Ther* 67:155–186.
28. Micheli V, et al. (2011) Neurological disorders of purine and pyrimidine metabolism. *Curr Top Med Chem* 11:923–947.
29. Formentini L, et al. (2009) Poly(ADP-ribose) catabolism triggers AMP-dependent mitochondrial energy failure. *J Biol Chem* 284:17668–17676.
30. Thompson LM, et al. (2009) IKK phosphorylates huntingtin and targets it for degradation by the proteasome and lysosome. *J Cell Biol* 187:1083–1099.
31. Shetty RS, et al. (2011) Specific correction of a splice defect in brain by nutritional supplementation. *Hum Mol Genet* 20:4093–4101.
32. Caron NS, Desmond CR, Xia J, Truant R (2013) Polyglutamine domain flexibility mediates the proximity between flanking sequences in huntingtin. *Proc Natl Acad Sci USA* 110:14610–14615.
33. Trettel F, et al. (2000) Dominant phenotypes produced by the HD mutation in STHdh(Q111) striatal cells. *Hum Mol Genet* 9:2799–2809.
34. Rajaram S, Pavie B, Wu LF, Altschuler SJ (2012) PhenoRipper: Software for rapidly profiling microscopy images. *Nat Methods* 9:635–637.
35. Axelrod FB, et al. (2011) Kinetin improves IKBKAP mRNA splicing in patients with familial dysautonomia. *Pediatr Res* 70:480–483.
36. Othman EM, Naseem M, Awad E, Dandekar T, Stopper H (2016) The plant hormone cytokinin confers protection against oxidative stress in mammalian cells. *PLoS One* 11: e0168386.
37. Jabłońska-Trypuć A, Matejczyk M, Czerpak R (2016) N6-benzyladenine and kinetin influence antioxidative stress parameters in human skin fibroblasts. *Mol Cell Biochem* 413:97–107.
38. Watkin EE, et al. (2014) Phosphorylation of mutant huntingtin at serine 116 modulates neuronal toxicity. *PLoS One* 9:e88284.
39. Slow EJ, et al. (2003) Selective striatal neuronal loss in a YAC128 mouse model of Huntington disease. *Hum Mol Genet* 12:1555–1567.
40. Niefind K, Pütter M, Guerra B, Issinger OG, Schomburg D (1999) GTP plus water mimic ATP in the active site of protein kinase CK2. *Nat Struct Biol* 6:1100–1103.
41. Pagano MA, et al. (2004) 2-Dimethylamino-4,5,6,7-tetrabromo-1H-benzimidazole: A novel powerful and selective inhibitor of protein kinase CK2. *Biochem Biophys Res Commun* 321:1040–1044.
42. Nuñez de Villavicencio-Diaz T, Rabalski AJ, Litchfield DW (2017) Protein kinase CK2: Intricate relationships within regulatory cellular networks. *Pharmaceuticals (Basel)* 10: E27.
43. Olsten MEK, Litchfield DW (2004) Order or chaos? An evaluation of the regulation of protein kinase CK2. *Biochem Cell Biol* 82:681–693.
44. Montenarh M (2016) Protein kinase CK2 in DNA damage and repair. *Transl Cancer Res* 5:49–63.
45. Tsutakawa SE, Lafrance-Vanasse J, Tainer JA (2014) The cutting edges in DNA repair, licensing, and fidelity: DNA and RNA repair nucleases sculpt DNA to measure twice, cut once. *DNA Repair (Amst)* 19:95–107.
46. Morales JC, Carpenter PB (2004) Breaking in a new function for casein kinase 2. *Sci Aging Knowledge Environ* 2004:pe24.
47. Guerra B, Iwabuchi K, Issinger O-G (2014) Protein kinase CK2 is required for the recruitment of 53BP1 to sites of DNA double-strand break induced by radiomimetic drugs. *Cancer Lett* 345:115–123.
48. Wyszko E, et al. (2003) "Action-at-a distance" of a new DNA oxidative damage product 6-furfuryl-adenine (kinetin) on template properties of modified DNA. *Biochim Biophys Acta* 1625:239–245.
49. Radhakrishna V, et al. (2017) Evaluation of the potency of kinetin on radiation induced behavioural changes in Swiss albino mice. *J Clin Diagn Res* 11:TF01–TF04.
50. Hickson I, et al. (2004) Identification and characterization of a novel and specific inhibitor of the ataxia-telangiectasia mutated kinase ATM. *Cancer Res* 64:9152–9159.
51. Fecke W, Gianfriddo M, Gaviraghi G, Terstappen GC, Heitz F (2009) Small molecule drug discovery for Huntington's disease. *Drug Discov Today* 14:453–464.
52. Kumar A, Ratan RR (2016) Oxidative stress and Huntington's disease: The good, the bad, and the ugly. *J Huntingtons Dis* 5:217–237.
53. Polyzos A, et al. (2016) Mitochondrial targeting of XJB-5-131 attenuates or improves pathophysiology in HdhQ150 animals with well-developed disease phenotypes. *Hum Mol Genet* 25:1792–1802.
54. Tilstra JS, et al. (2014) Pharmacologic IKK/NF-κB inhibition causes antigen presenting cells to undergo TNFα dependent ROS-mediated programmed cell death. *Sci Rep* 4: 3631.
55. Wei Y, et al. (2017) Neuroprotective effects of kinetin against glutamate-induced oxidative cytotoxicity in HT22 cells: Involvement of Nrf2 and heme oxygenase-1. *Neurotox Res* 33:725–737.
56. Wei Y, et al. (2017) Protective effects of kinetin against aluminum chloride and D-galactose induced cognitive impairment and oxidative damage in mouse. *Brain Res Bull* 134:262–272.
57. Saudou F, Finkbeiner S, Devys D, Greenberg ME (1998) Huntingtin acts in the nucleus to induce apoptosis but death does not correlate with the formation of intranuclear inclusions. *Cell* 95:55–66.
58. Kratter IH, et al. (2016) Serine 421 regulates mutant huntingtin toxicity and clearance in mice. *J Clin Invest* 126:3585–3597.
59. Warby SC, et al. (2009) Phosphorylation of huntingtin reduces the accumulation of its nuclear fragments. *Mol Cell Neurosci* 40:121–127.
60. Arbez N, et al. (2017) Post-translational modifications clustering within proteolytic domains decrease mutant huntingtin toxicity. *J Biol Chem* 292:19238–19249.
61. Sorrentino V, et al. (2017) Enhancing mitochondrial proteostasis reduces amyloid-β proteotoxicity. *Nature* 552:187–193.
62. Sakaguchi K, et al. (1997) Phosphorylation of serine 392 stabilizes the tetramer formation of tumor suppressor protein p53. *Biochemistry* 36:10117–10124.
63. Correia K, et al. (2015) The Genetic Modifiers of Motor OnsetAge (GeM MOA) website: Genome-wide association analysis for genetic modifiers of Huntington's disease. *J Huntingtons Dis* 4:279–284.
64. Herhaus L, et al. (2015) Casein kinase 2 (CK2) phosphorylates the deubiquitylase OTUB1 at Ser16 to trigger its nuclear localization. *Sci Signal* 8:ra35.
65. Barciszewski J, Siboska GE, Pedersen BO, Clark BF, Rattan SI (1997) A mechanism for the in vivo formation of N6-furfuryladenine, kinetin, as a secondary oxidative damage product of DNA. *FEBS Lett* 414:457–460.
66. Schütt F, Aretz S, Auffarth GU, Kopitz J (2012) Moderately reduced ATP levels promote oxidative stress and debilitate autophagic and phagocytic capacities in human RPE cells. *Invest Ophthalmol Vis Sci* 53:5354–5361.
67. Mochel F, Haller RG (2011) Energy deficit in Huntington disease: Why it matters. *J Clin Invest* 121:493–499.
68. Nath S, Munsie LN, Truant R (2015) A huntingtin-mediated fast stress response halting endosomal trafficking is defective in Huntington's disease. *Hum Mol Genet* 24: 450–462.
69. Vishnu N, et al. (2014) ATP increases within the lumen of the endoplasmic reticulum upon intracellular Ca2+ release. *Mol Biol Cell* 25:368–379.
70. Vidal R, Caballero B, Couve A, Hetz C (2011) Converging pathways in the occurrence of endoplasmic reticulum (ER) stress in Huntington's disease. *Curr Mol Med* 11:1–12.
71. Jiang B, Glover JNM, Weinfeld M (2017) Neurological disorders associated with DNA strand-break processing enzymes. *Mech Ageing Dev* 161:130–140.
72. Turowec JP, et al. (2010) Protein kinase CK2 is a constitutively active enzyme that promotes cell survival: Strategies to identify CK2 substrates and manipulate its activity in mammalian cells. *Methods Enzymol* 484:471–493.
73. Frank R (2002) The SPOT-synthesis technique. Synthetic peptide arrays on membrane supports–Principles and applications. *J Immunol Methods* 267:13–26.
74. Duncan JS, et al. (2011) A peptide-based target screen implicates the protein kinase CK2 in the global regulation of caspase signaling. *Sci Signal* 4:ra30.
75. Porsolt RD, Le Pichon M, Jalfre M (1977) Depression: A new animal model sensitive to antidepressant treatments. *Nature* 266:730–732.
76. Wanker EE, et al. (1999) Membrane filter assay for detection of amyloid-like polyglutamine-containing protein aggregates. *Methods Enzymol* 309:375–386.